NaCl-template-based Synthesis of TiO_2-Pd/Pt Hollow Nanospheres for H_2O_2 Direct Synthesis and CO Oxidation

Mareike Liebertseder[a], Di Wang[b], Gülperi Cavusoglu[c], Maria Casapu[c], Sheng Wang[d], Silke Behrens[d], Christian Kübel[b], Jan-Dierk Grunwaldt[c,d], and Claus Feldmann[a]*

[a]Institute of Inorganic Chemistry (IAC), Karlsruhe Institute of Technology (KIT), Engesserstraße 15, D-76131 Karlsruhe (Germany), E-mail: claus.feldmann@kit.edu

[b]Institute of Nanotechnology (INT), Karlsruhe Institute of Technology (KIT), Hermann-von-Helmholtz-Platz 1, 76344 Eggenstein-Leopoldshafen (Germany)

[c]Institute for Chemical Technology and Polymer Chemistry (ICTP), Engesserstraße 20, 76131 Karlsruhe (Germany)

[d]Institute of Catalysis Research and Technology (IKFT), Karlsruher Institute of Technology (KIT), Hermann-von-Helmholtz-Platz 1, 76344 Eggenstein-Leopoldshafen (Germany)

– Supporting Information –

Content:

1. Analytical Techniques

Transmission electron microscopy (TEM). TEM was conducted with two microscopes. NaCl@TiO_2 core-shell nanoparticles were characterized on a FEI Osiris microscope operated at 200 kV. TiO_2-Pd HNS and TiO_2-Pt HNS samples were characterized on an aberration (image) corrected FEI Titan 80-300 microscope operated at 300 kV. The FEI Osiris microscope was equipped with a Bruker Quantax system (XFlash detector). The FEI Titan 80-300 microscope was equipped with a Fishione model 3000 HAADF-STEM detector and EDAX s-UTW EDX detector. EDX spectra were quantified with the FEI software package "TEM imaging and analysis" (TIA). TEM samples were prepared by putting a drop of suspension of the respective powder sample in ethanol onto a copper grid coated with amorphous carbon (Lacey-) supporting film. Average particle diameters were calculated by statistical evaluation of at least 150 nanoparticles (ImageJ 1.47v software).

Electron tomography was performed using a Fishione 2020 tomography holder on an FEI Titan 80-300 microscope in STEM mode with a nominal beam diameter of 0.27 nm. HAADF STEM tilt series with image dimensions of 1024×1024 pixels were collected using the Xplore3D software (FEI) over a tilt range of at least ±76°, with tilt increments of 2°. Alignment of the tilt series was performed with IMOD using supported Pd nanoparticles as fiducial markers, with the final alignment residual mean error being 0.52 pixel. The aligned tilt series were reconstructed using the simultaneous iterative reconstruction technique (SIRT) within Inspect3D (FEI). 3D structure rendering was performed using Amira 6.0 (FEI) software.

X-ray powder diffraction (XRD). X-ray powder diffraction (XRD) was performed with a Stoe STADI-MP diffractometer operating with Ge-monochromatized Cu-$K\alpha$-radiation (λ = 1.54178 Å) and Debye-Scherrer geometry. The dried samples were fixed between Scotch tape and acetate paper and measured between -69° and +69° of two-theta.

Volumetric sorption analysis was carried out with an AUTOSORB IQ-XR VITON (Anton Paar), applying N_2 as adsorbate. Specific surface area was determined using Brunauer-Emmett-Teller (BET) theory, pore analysis was performed using density functional theory (DFT) methods, respectively.

Gravimetric CO_2 and N_2 sorption analysis were carried out with an IsoSORP Static magnetic suspension balance (Rubotherm) that can be operated up to 200 bar. The significance of the

balance was ≤0.1 mg. Thus, a stainless steel sample holder was filled with the powder sample and placed at the balance coupling under inert gas flow in order to prevent contact with air and moisture. Subsequently, the balance was evacuated for 6 h at 333 K and 10^{-3} mbar until constant mass was achieved. Afterwards, the gas was dosed into the balance chamber to elevated pressures. Equilibrium was achieved within 30 min to 2 h and identified by constant weight and pressure. The temperature was kept constant with an accuracy of ±0.5 K for each measurement. Additionally, a helium buoyancy correction was used to calculate the surface excess mass from the measured values.

2. Experimental Details of Direct Synthesis of H_2O_2

Catalytic tests for H_2O_2 direct synthesis were carried out in a semi-continuous batch reactor at 30 °C and 40 bar. The reactor (300 mL) was equipped with a Teflon inlay, mechanical blowing stirrer (Teflon), and Teflon baffles. The catalysts (1.3 mg Pd) were suspended in ethanol (200 mL) and activated with 4 vol% H_2 in N_2 (250 mL_{NTP} min^{-1}). The reaction gas mixture (total flow 250 mL_{NTP} min^{-1}, gas composition $H_2 : O_2 : N_2 = 4 : 20 : 76$) was introduced and stirring was started (1000 rpm). The H_2, O_2, and N_2 concentrations were analyzed online at the reactor outlet by GC (Inficon micro GC 3000). N_2 was used as internal standard to calculate the H_2 and O_2 concentrations. The H_2O_2 concentration was quantified using $TiO(SO_4)/H_2SO_4$ and UV/Vis spectroscopy (Specord S600, Analytik Jena). The H_2 conversion ($X(H_2)$) and H_2O_2 selectivity ($S(H_2O_2)$) were determined after 63 min of the reaction according to equations (1) and (2), respectively. Catalytic tests were repeated and mean values were calculated.

$$X(H_2) = \frac{Consumed\ H_2\ (mol)}{Inlet\ H_2\ (mol)} \times 100\% \quad (1)$$

$$S(H_2O_2) = \frac{n(H_2O_2)\ (mol)}{H_2\ consumed\ (mol)} \times 100\% \quad (2)$$

The determination of the H_2O_2 concentration was performed according to the following procedure. The concentration of a commercial H_2O_2 solution (approximately 27.42 wt-%) was titrated with an aqueous $KMnO_4$ solution (0.02 M). A solution of $TiOSO_4/H_2SO_4$ (2 wt-%, 1 L) was prepared by dissolving titanium(IV) oxysulfate - sulfuric acid hydrate (85 g) in H_2SO_4 (20 wt-%, 1 L). The solution was stirred overnight und filtrated before use. Initially, a H_2O_2 stock solution (35 mM) was prepared in a 50 mL volumetric flask by diluting the commercial H_2O_2 solution with water. 1 mL of the $TiOSO_4/H_2SO_4$ solution was then added to a corresponding quantity of the H_2O_2 stock solution and diluted with H_2SO_4 (0.03 M) to 50 mL

in a volumetric flask. To establish the calibration curve, the absorbance of the orange-yellow peroxo complex was determined in a H_2O_2 concentration range from 0.0441 to 1.05 mmol/L in a cuvette (d = 1 cm) at a wavelength of 420 nm using a Specord S600 (Analytik Jena) (Figure S1). In the catalytic tests, a sample of the reaction mixture was taken every 9 min and the catalyst removed by centrifugation. 1 mL of the reaction mixture and 1 mL of $TiOSO_4/H_2SO_4$ (2 wt-%) were then placed in a volumetric flask and diluted with aqueous H_2SO_4 solution (0.03 M) to the calibration range.

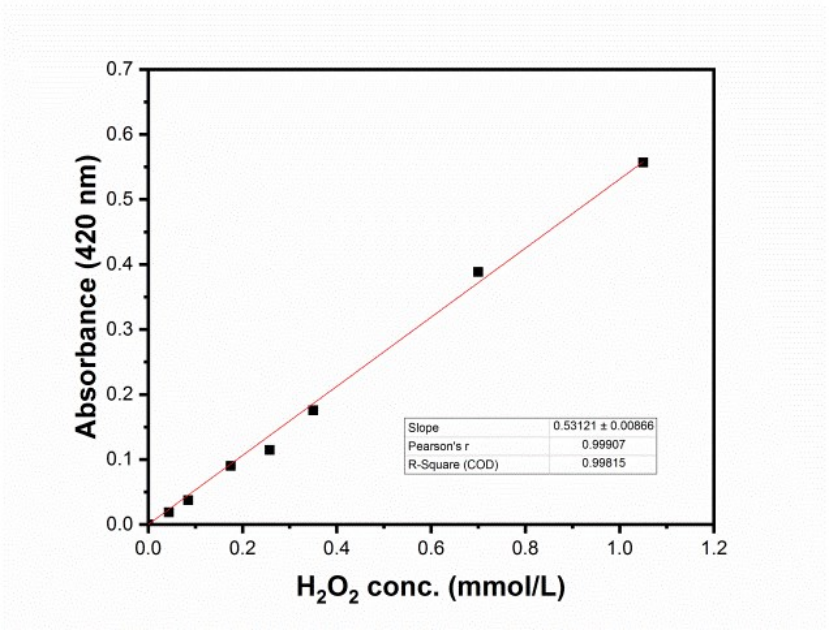

Figure S1. Calibration curve to determine the H_2O_2 concentration by UV-Vis spectrometry.

For catalytic activity tests of the CO oxidation, TiO_2-Pt HNS (0.7 wt-%) were used as sieved granulate fractions (125-250 µm). Thereafter, CO oxidation was performed in quartz microreactors (inner diameter: 1.5 mm) at atmospheric pressure at 30-400 °C (heating rate: 5 °C/min). The gas mixture (1000 ppm CO, 10% O_2 in He) was applied with a total gas flow of 50 mL/min (GHSV: 60.000 h^{-1}). Thereafter, the gas composition was detected by mass spectrometry (Pfeiffer Thermostar) at the reactor outlet (CO consumption, CO_2 formation).

3. Synthesis Details

The course of the reaction starting with a THF solution, followed by the formation of the nanosized NaCl template, the deposition of the TiO_2 shell with formation of a NaCl@TiO_2 core-shell structure and the final formation of TiO_2 HNS can be followed with the naked eye (Figure S2). The photos also indicate the stability of the suspensions throughout the course of

the synthesis. Moreover, they qualitatively illustrate the increasing particle size, which correlates to the turbidity of the respective suspension.

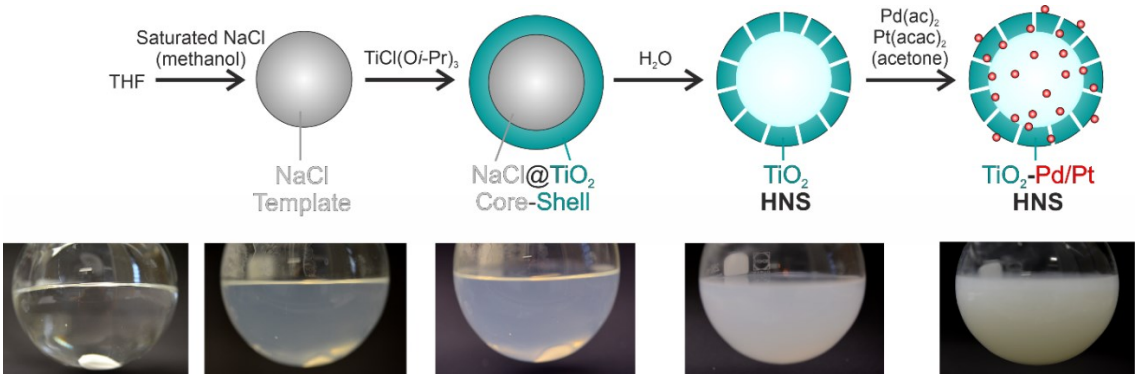

Figure S2. Schematic one-pot synthesis of TiO_2-Pd/Pt hollow nanospheres (HNS) via NaCl templates with photos to illustrate the course of the reaction.

4. Materials Characterization: TiO_2 HNS

If the deposition of TiO_2 on the NaCl template was performed with addition of Ti(O*n*-Bu)$_4$, the speed of hydrolysis turned out to be too slow (*see discussion in main text*). As a result, only fluffy TiO_2 with incomplete coverage of the NaCl template was obtained (Figure S3a,b). EDXS line scans nevertheless clearly prove the presence of hollow structures after removal of the NaCl template (Figure S3c,d). A much more controlled deposition of the NaCl template was possible upon injection of TiCl(O*i*-Pr)$_3$, which results in a uniform TiO_2 layer on the NaCl template (*see main text: Figures 1,3,4*).

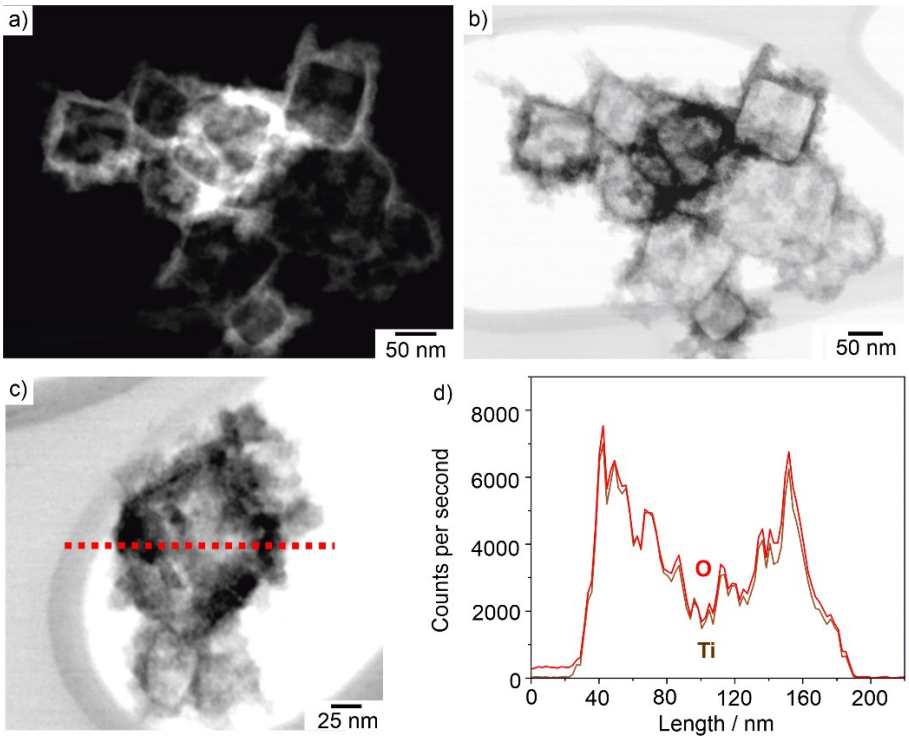

Figure S3. Fluffy TiO_2 after hydrolysis of Ti(O*n*-Bu)$_4$: a+b) Electron microscopy at different levels of magnification; c+d) EDXS line scan (d) along the dotted red line in (c).

Volumetric sorption analysis allows determining the specific surface area (according to the Brunauer-Emmett-Teller/BET formalism) and the pore volume (according to density functional theory/DFT methods). The resulting data are summarized in the main text (*see main text: Table 1*). In addition, the pore diameter was analyzed (Figure S4). Accordingly, the as-prepared fluffy TiO_2 (with Ti(O*n*-Bu)$_4$ precursor) and the as-prepared TiO_2 HNS (with TiCl(O*i*-Pr)$_3$ precursor) show comparable features with very small pores (≤8 Å) and larger pores in the 10-20 Å range. Hereof, the smaller pores are more dominant for fluffy TiO_2 (with Ti(O*n*-Bu)$_4$ precursor) in comparison to the TiO_2 HNS (with TiCl(O*i*-Pr)$_3$ precursor).

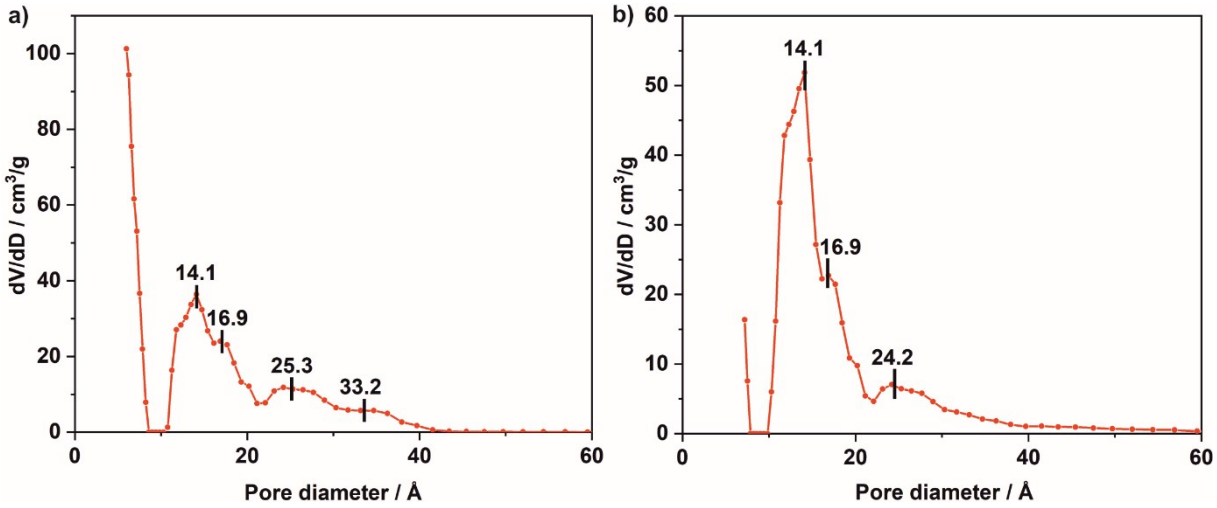

Figure S4. Pore diameter of as-prepared TiO_2: a) fluffy TiO_2 (with Ti(O*n*-Bu)$_4$ precursor); b) TiO_2 HNS (with TiCl(O*i*-Pr)$_3$ precursor).

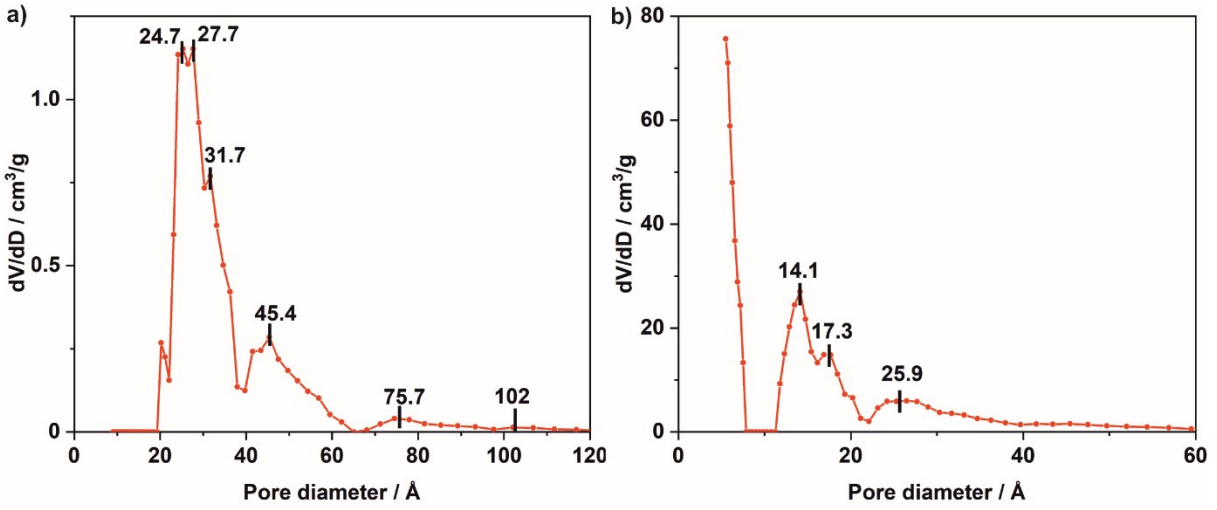

Figure S5. Pore diameter of sintered TiO_2 (300 °C, N_2): a) fluffy TiO_2 (with Ti(O*n*-Bu)$_4$ precursor); b) TiO_2 HNS (with TiCl(O*i*-Pr)$_3$ precursor).

Subsequent to sintering (300 °C, N_2), however, the pore diameter of fluffy TiO_2 (with Ti(O*n*-Bu)$_4$ precursor) was shifted to significantly larger values of 20-40 Å (Figure S5a), whereas the pore diameters of the TiO_2 HNS (with TiCl(O*i*-Pr)$_3$ precursor) remained similar with more pronounced very small pores (≤8 Å, Figure S5b). This behavior is similar to the observation related to the specific surface area and the pore volume (*see main text: Table 1*).

Volumetric sorption analysis of TiO_2 HNS, which was performed with nitrogen, clearly shows type II isotherms (Figure S6a). In addition to volumetric sorption analysis, gravimetric sorption analysis was performed for TiO_2 HNS up to pressures of 80 bar (Figure S6b). Here, the high surface area and the high porosity were confirmed for CO_2 and N_2 as sorbents. Moreover, the TiO_2 HNS show considerable CO_2 uptake of about 200 mg/g (Figure S6b). In comparison, the N_2 uptake is significantly lower and reaches about 30 mg/g at 80 bar. Consequently, the TiO_2 HNS also show certain selectivity of CO_2 adsorption over N_2 adsorption.

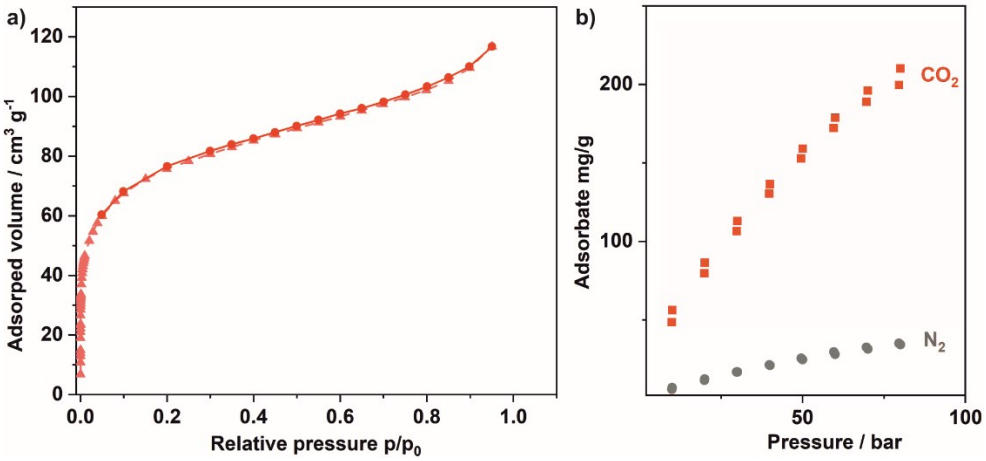

Figure S6. Sorption analysis of TiO_2 HNS: a) Volumetric N_2 sorption/desorption; b) Gravimetric N_2 and CO_2 adsorption/desorption isotherms at elevated pressure.

Finally, the crystallinity and phase composition of the TiO_2 HNS was analyzed by X-ray powder diffraction (XRD) (Figure S7). Thus, the as-prepared TiO_2 HNS are amorphous and did not show any Bragg peak (Figure S7a). After sintering (300 °C, N_2), well-defined Bragg peaks become visible and point to the presence of TiO_2 with the anatase modification (Figure S7b).

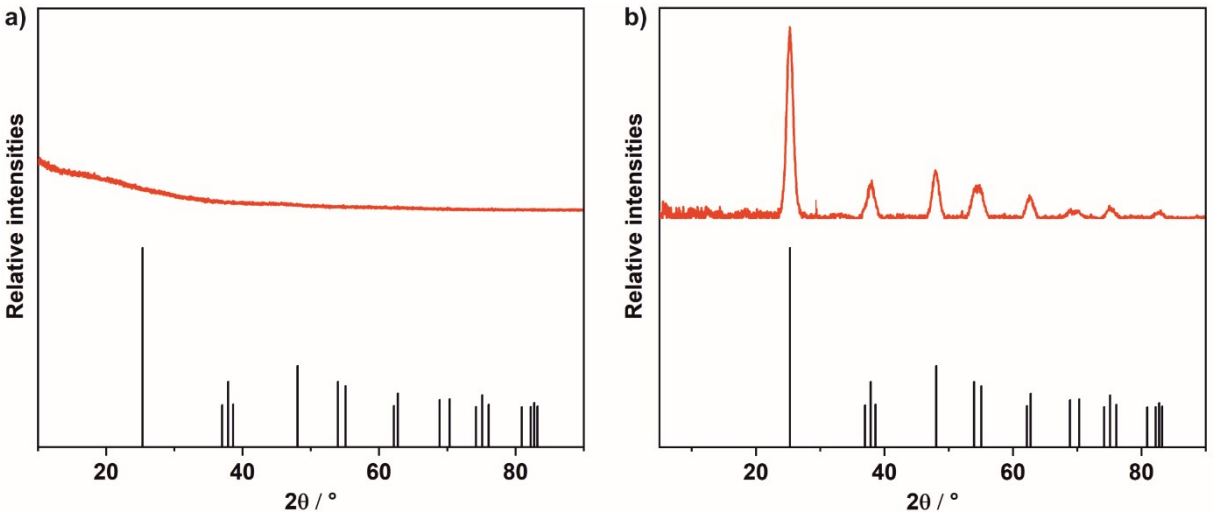

Figure S7. Powder diffraction patterns of TiO_2 HNS: a) As-prepared, b) after sintering at 300 °C in nitrogen (reference: ICDD-No. 086-1157, anatase).

5. Materials Characterization: TiO_2-Pd HNS

High-resolution transmission electron microscopy (HR-TEM) and energy-dispersive X-ray spectroscopy (EDXS) of the as-prepared TiO_2-Pd HNS (5 wt-%) validate the hollow-sphere structure and clearly display the inner cavity (Figure S8a-c; *see main text: Figure 5*). Pd nanoparticles are deposited all over the TiO_2 HNS, including outer and inner surface of the HNS, as revealed by electron tomography. A slice image from the reconstructed 3D volume is shown in Figure S9. The TiO_2-Pd HNS show larger Pd agglomerates up to about 10 nm as well as very small Pd nanoparticles, 3-7 nm in size (Figure S8b,d,e). The broader size distribution of Pd on TiO_2-Pd HNS (5 wt-%) in comparison to the size distribution of Pt on TiO_2-Pt HNS (0.7 wt-%) (*see Figures S13-S15*) can be predominately ascribed to the higher concentration of Pd.

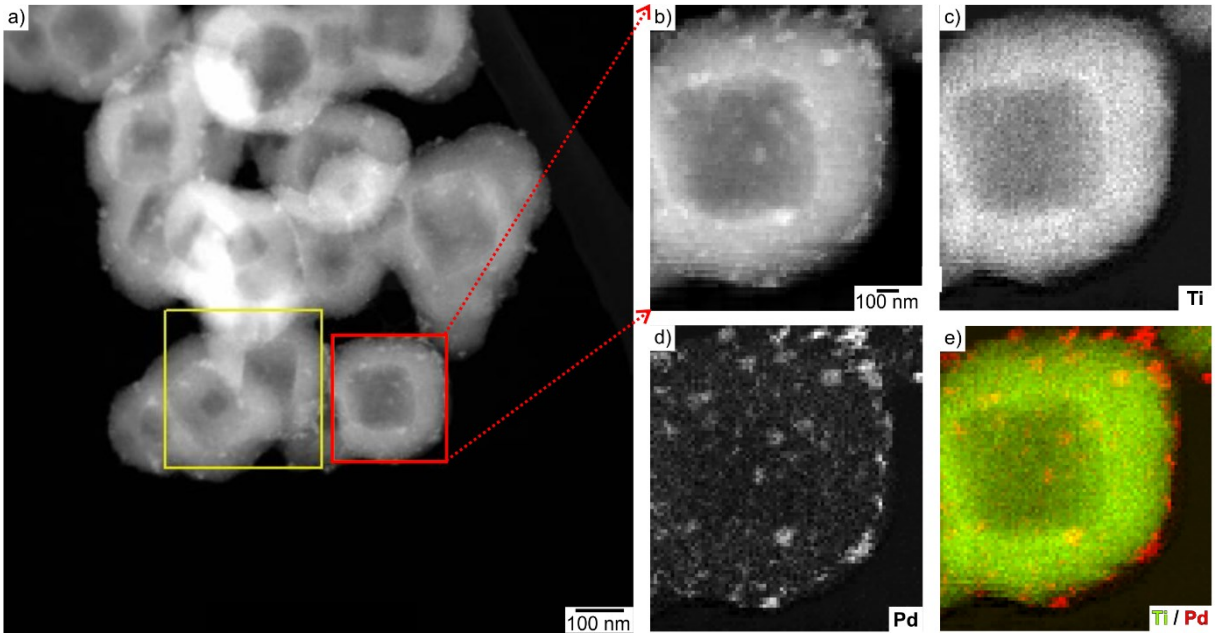

Figure S8. TiO_2-Pd HNS (5 wt-% Pd) for H_2O_2 direct synthesis (as-prepared): a) Overview image; b) High-resolution image; c+d) EDXS element mapping of TiO_2-Pd HNS on (b) with Ti (c) and Pd (d); e) Overlay of Ti and Pd element mappings.

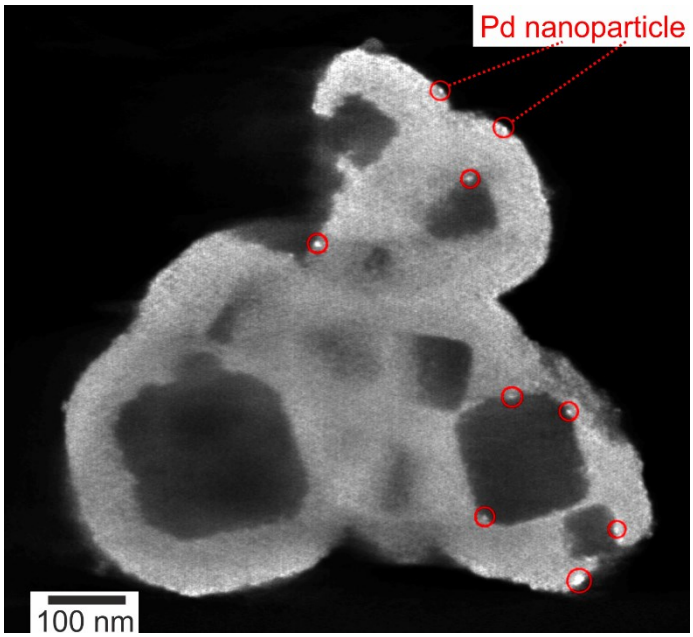

Figure S9. Slice view from electron tomogram of TiO_2-Pd HNS (5 wt-% Pd) for H_2O_2 direct synthesis (as-prepared) with some selected Pd nanoparticles indicated by red circles.

In addition to the pore diameter of the as-prepared TiO_2 HNS (Figure S4b), the pore diameter was analyzed after impregnation with Pd (Figure S10). Whereas specific surface area and pore volume were reduced by about 40% upon deposition of Pd (*see main text: Table S1*), the pore diameter is almost unaffected and mainly shows pores in the 10-20 Å range (Figure S10).

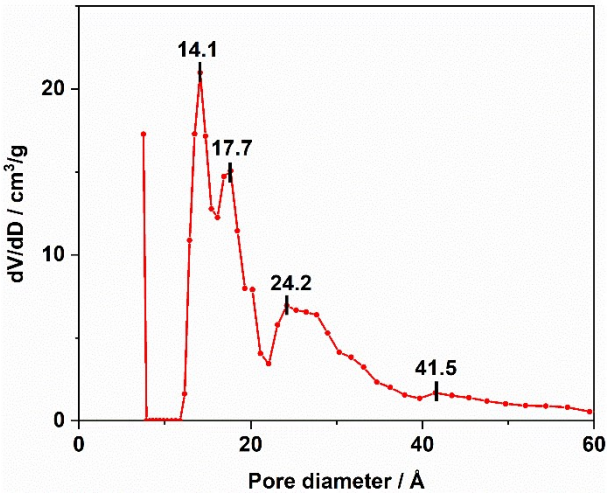

Figure S10. Pore diameter of the as-prepared TiO_2-Pd HNS (5 wt-%).

By statistical evaluation of TEM images, moreover, the size distribution of the Pd nanoparticles of TiO_2-Pd HNS (5 wt-%) was examined (Figure S11). This results in a size distribution of 2-10 nm. Most of the Pd nanoparticles exhibit a size of 3-7 nm.

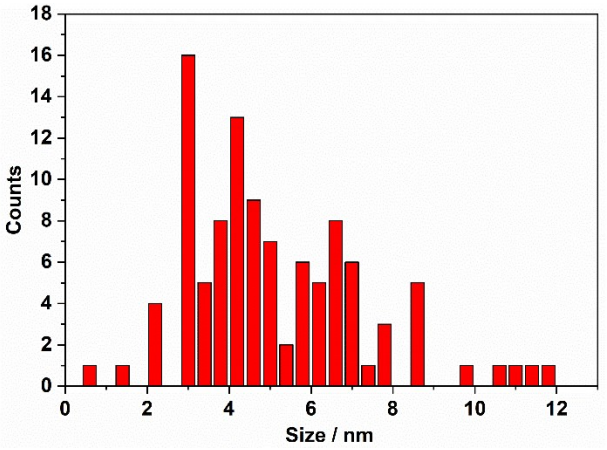

Figure S11. Size distribution of Pd nanoparticles of the as-prepared TiO_2-Pd HNS (5 wt-%).

HRTEM images and selected area electron diffraction (SAED) were performed to analyze the crystallinity and phase composition of the as-prepared TiO_2-Pd HNS (5 wt-%) (Figures S12,S13). Here, TiO_2 was found with a mixture of nanocrystalline and amorphous nanoparticles (Figure S12a,b). The crystalline TiO_2 domains clearly show parallel lattice fringes in areas about 1-4 nm in size (Figure S12a,b). The fast Fourier transformations (FFTs) of selected crystalline TiO_2 domains point to the presence of the anatase phase (Figure S12d,e). Since the as-prepared TiO_2-Pd HNS were treated at 70 °C as the highest temperature during drying, the observation of crystalline TiO_2 is surprising either way and can be ascribed to the

well-controlled conditions of nucleation. Furthermore, HRTEM images indicate the Pd nanoparticles as expected to be highly crystalline (Figure S12c,e). Based on a radial distribution function (RDF) analysis of the SAED data, the short-range order (chemical nature) of the amorphous TiO_2 is dominated by the anatase phase (Figure S13).

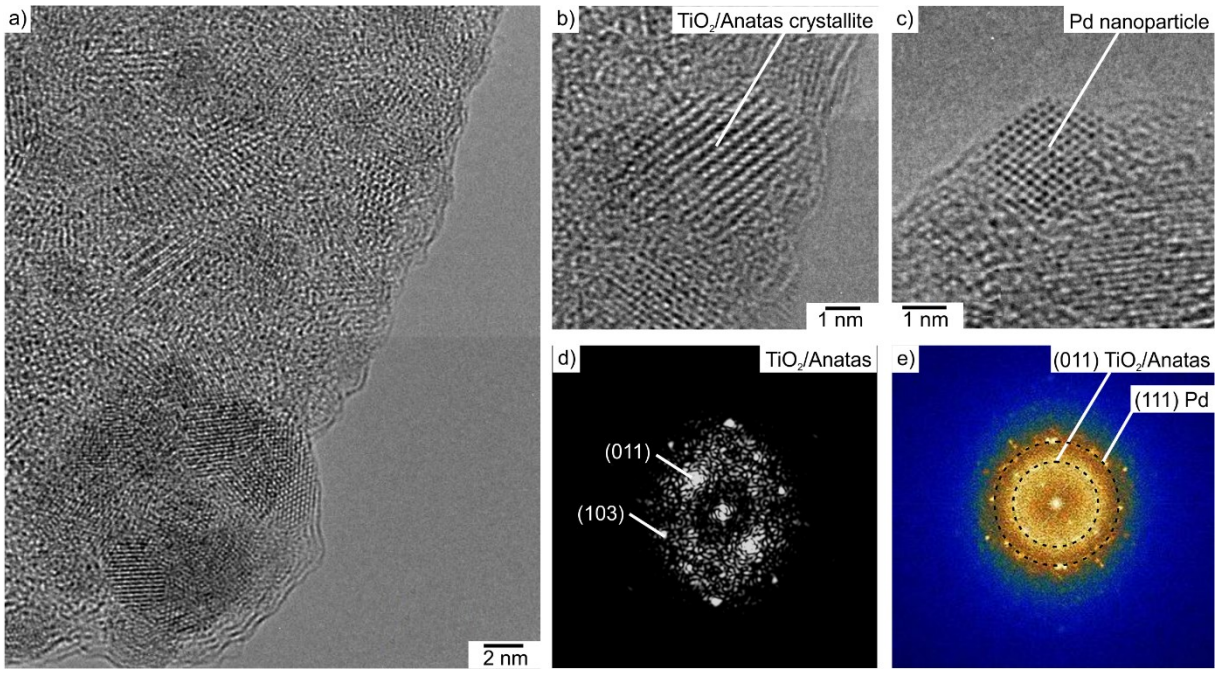

Figure S12. Crystallinity and phase analysis of the as-prepared TiO_2-Pd HNS (5 wt-%): a) Overview image with crystalline and amorphous TiO_2; b) HRTEM of crystalline TiO_2 domain; c) HRTEM of crystalline Pd nanoparticle; d) SAED of crystalline TiO_2 domain; e) FFT of crystalline TiO_2 domain along (31-1) zone axis.

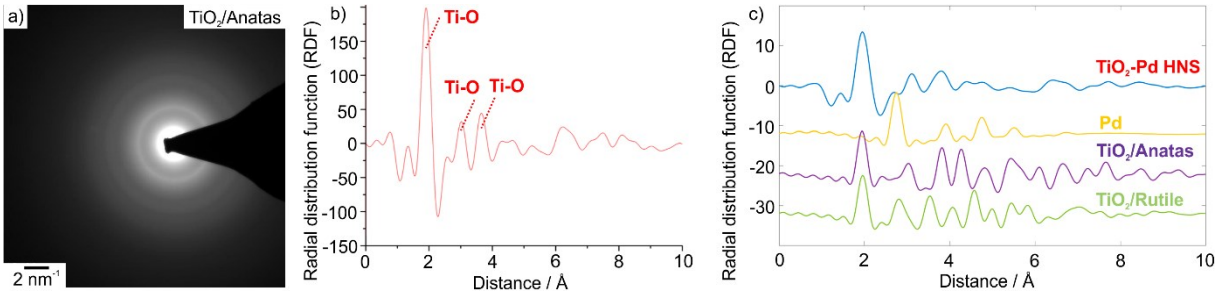

Figure S13. Crystallinity and phase analysis of the as-prepared TiO_2-Pd HNS (5 wt-%): a) SAED; b) RDF analysis of Ti–O and Ti–Ti distances; c) Comparison of RDF analysis in (b) with reference data.

Subsequent to its use for H_2O_2 direct synthesis, the TiO_2-Pd HNS (5 wt-%) were separated from the aqueous suspension by centrifugation, and the structure of the catalyst was again

examined by TEM and EDXS (Figure S14). In regard of the conditions of H_2O_2 formation (i.e. acidic aqueous suspension, 30 bar, 30 °C, *see SI: section 2.*), partial dissolution of TiO_2 with Ostwald ripening and formation of dense TiO_2 nanoparticles could be expected. However, TEM clearly shows the presence of the HNS structure after the catalytic reaction (Figure S14a,c). Due to the low temperature of 30 °C, sintering effects and a growth of the Pd nanoparticles are a lower risk in comparison to the catalytic CO oxidation performed at up to 400 °C. Accordingly, TEM and EDXS confirm a uniform distribution of small-sized Pd nanoparticles all over the TiO_2 HNS after H_2O_2 direct synthesis (Figure S14b,d).

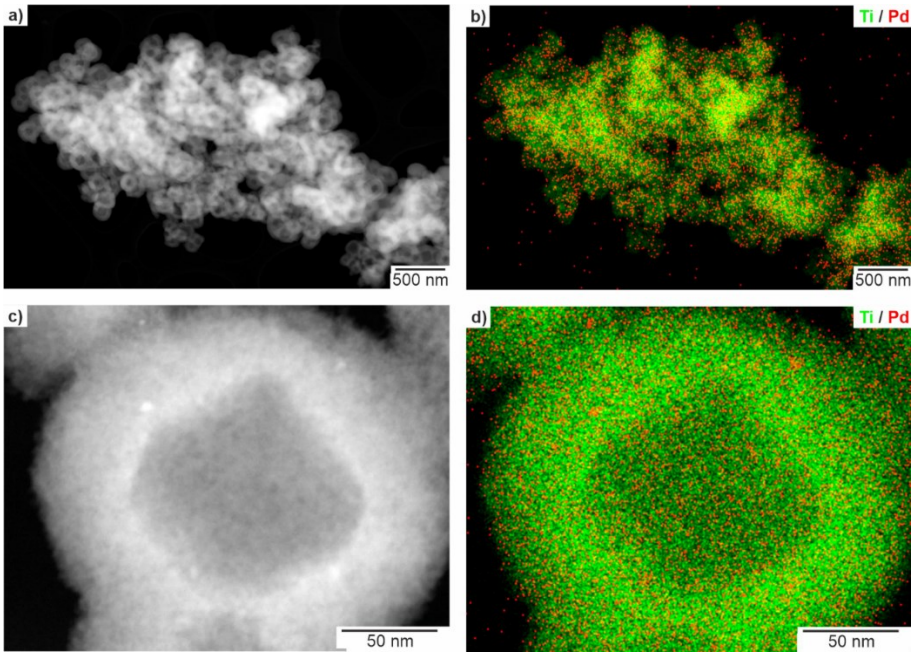

Figure S14. TiO_2-Pd HNS (5 wt-% Pd) after H_2O_2 direct synthesis: a) Overview image; c) High-resolution image; b+d) EDXS element mapping with Ti (green) and Pd (red) element mappings.

6. Materials Characterization: TiO_2-Pt HNS

Due to the fact that CO oxidation was performed at elevated temperature (20-300 °C), first of all, the size distribution and stability of the Pt nanoparticles were examined for the as-prepared TiO_2-Pt HNS (0.7 wt-%) as well as for samples sintered at 300 °C in nitrogen (Figure S15). HRTEM images and EDXS of the as-prepared TiO_2-Pt HNS (0.7 wt-%) again validate the hollow-sphere structure and clearly display the inner cavity (Figure S15; *see main text: Figure 6*). Similar to TiO_2-Pd HNS, Pt nanoparticles are deposited all over the TiO_2 HNS, including outer and inner surface as well as the pores through the HNS wall. The Pt

nanoparticles exhibit small particle sizes of 3-4 nm. Most interestingly, the size and size distribution prior and after sintering are very comparable (Figure S15; *see main text: Figure 6*). The finding of highly dispersed Pt nanoparticles was also confirmed by high-resolution EDXS images of sintered TiO_2-Pt HNS (Figure S16), which indicates the presence of very small Pt nanoparticles all over the TiO_2 HNS also after sintering at 300 °C in nitrogen.

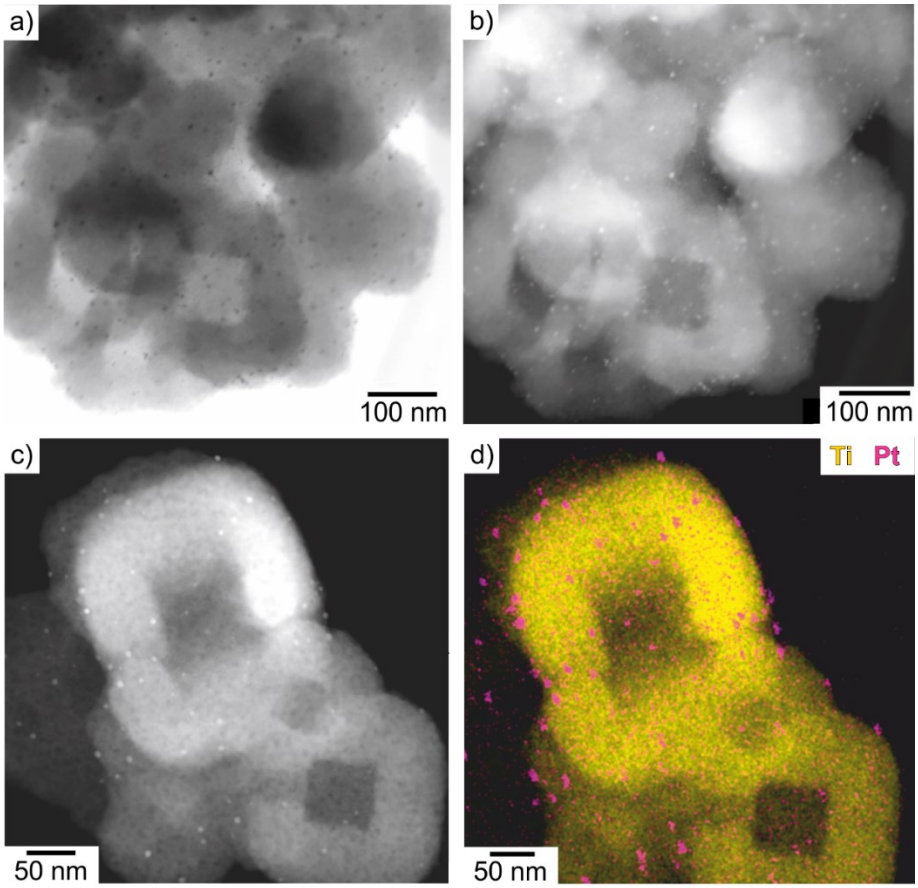

Figure S15. TiO_2-Pt HNS (0.7 wt-%) before (a,b) and after sintering (300 °C, N_2) (c) with EDXS analysis after sintering (d).

In addition to the pore diameter of the as-prepared TiO_2 HNS (Figure S3b), the pore diameter was analyzed after impregnation with Pt (Figure S17a) as well as after sintering at 300 °C in nitrogen (Figure S17b). The TiO_2-Pt HNS show about 35% reduction of the specific surface are and pore volume after the deposition of the Pt nanoparticles and about 20% reduction of specific surface area due to sintering at 300 °C (*see main text: Table S1*). Such loss of specific surface area and pore volume was also observed after the deposition of Pd nanoparticles. After deposition of Pt, the pore diameter predominately shows values <8 Å and of 10-20 Å (Figure S17a). These pores are also available after sintering (300 °C, N_2), however, with an additional fraction of pores with a diameter of 25-40 Å (Figure S17b).

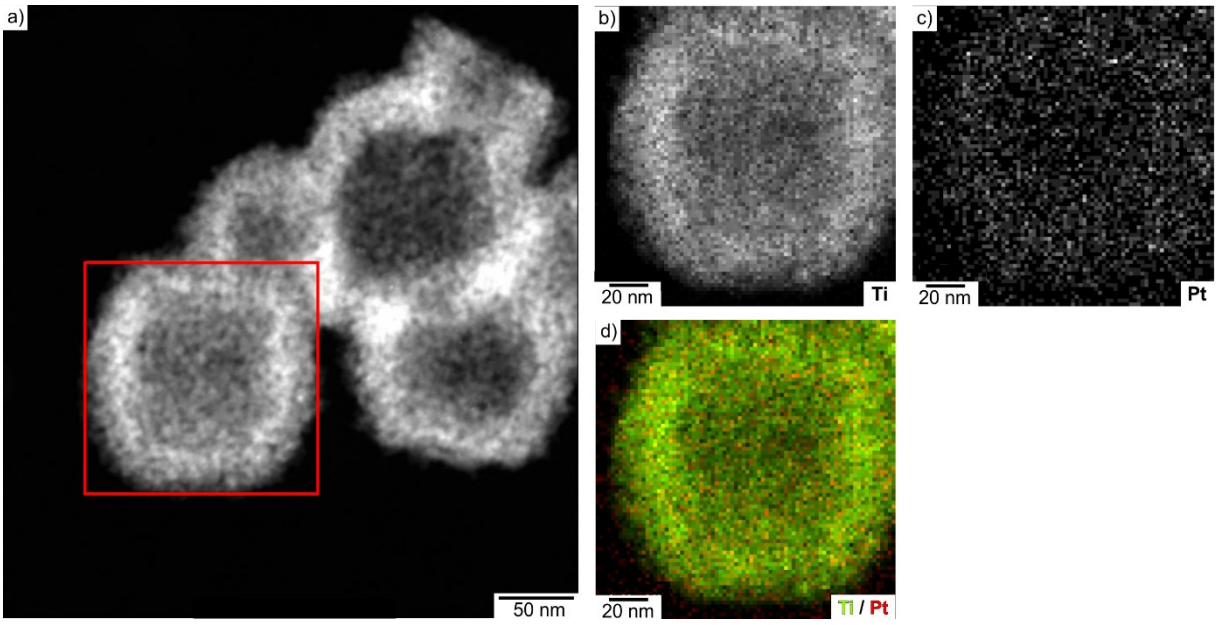

Figure S16. TiO_2-Pt HNS (0.7 wt-% Pt) for CO oxidation (sintered at 300 °C, N_2): a) Overview image; b+c) EDXS element mapping of TiO_2-Pt HNS on (a) with Ti (b) and Pt (c); d) Overlay of Ti and Pt element mappings.

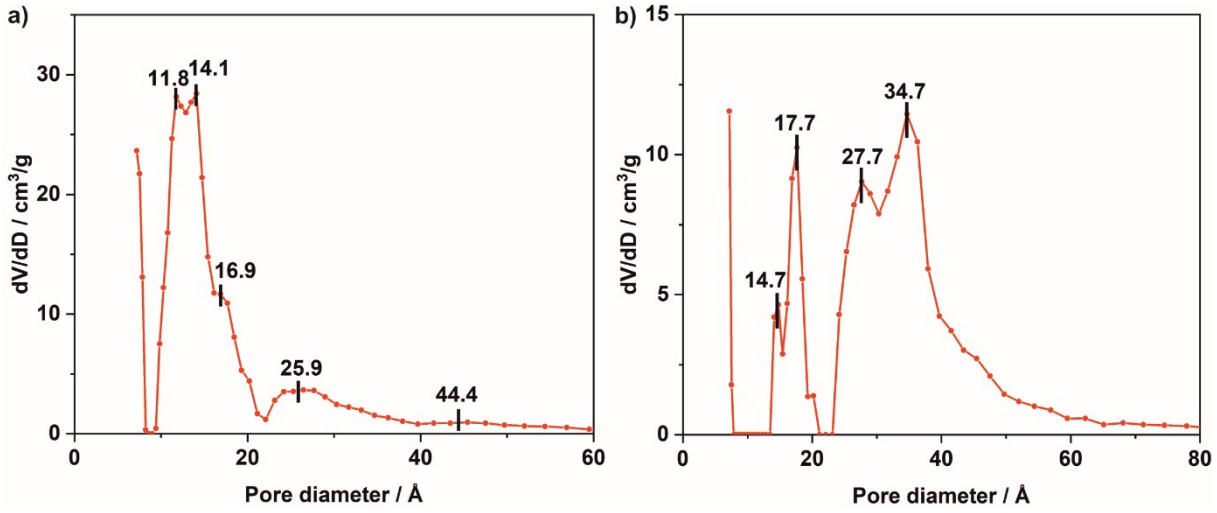

Figure S17. Pore diameter of TiO_2-Pt (0.7 wt-%) after preparation (a) and after sintering (300 °C, N_2) (b).

By statistical evaluation of TEM images, moreover, the size distribution of the Pt nanoparticles of TiO_2-Pt HNS (0.7 wt-%) was examined (Figure S18). This results in a size distribution of 2 to 7 nm after impregnation (Figure S18a), which remains almost unaffected after sintering at 300 °C in nitrogen (Figure S18b). Most interestingly, the size and size distribution prior and after sintering are very comparable (Figure S15; *see main text: Figure 6*). These findings are in agreement with TEM images (Figure S15) and were also confirmed by

high-resolution EDXS images of sintered TiO_2-Pt HNS (Figure S16), which indicates the presence of small Pt nanoparticles all over the TiO_2 HNS after sintering at 300 °C in nitrogen.

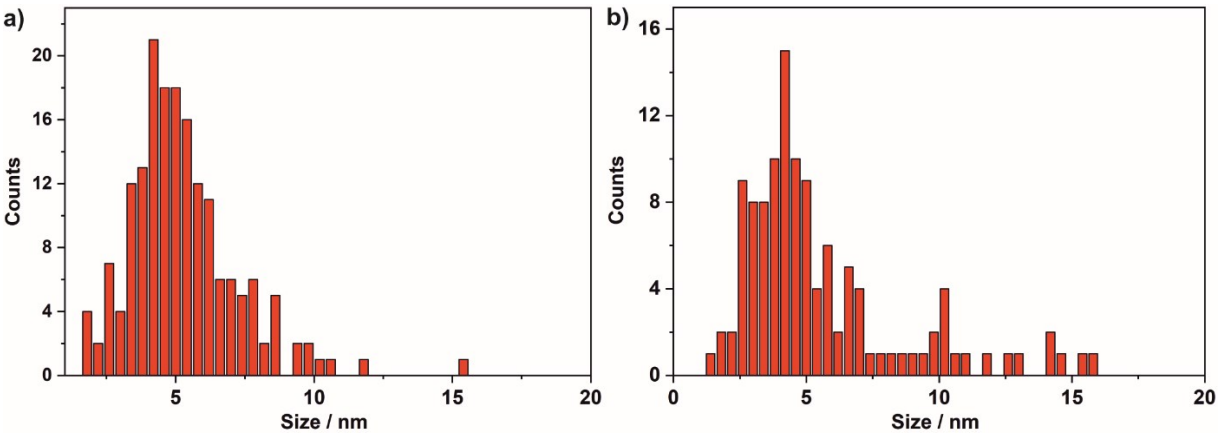

Figure S18. Size distribution of Pt nanoparticles of TiO_2-Pt HNS (0.7 wt-%) after preparation (a) and after sintering (300 °C, N_2) (b).

HRTEM images and SAED patterns of sintered TiO_2-Pt HNS (0.7 wt-%) clearly show crystalline TiO_2 domains (Figure S19a,b). After sintering, the TiO_2 HNS are expected to be much more crystalline than the as-prepared TiO_2 HNS. The crystalline TiO_2 domains are nevertheless still small with a size range of about 5-10 nm (Figure S19a). SAED shows Bragg reflections that can be indexed as anatase (Figure S19b,c). Similar to Pd in TiO_2-Pd HNS, the Pt nanoparticles can be also expected to be crystalline. Due to their very small size (3-4 nm) and low loading, however, their scattering power is very low and cannot be detected in the SAED patterns shown here.

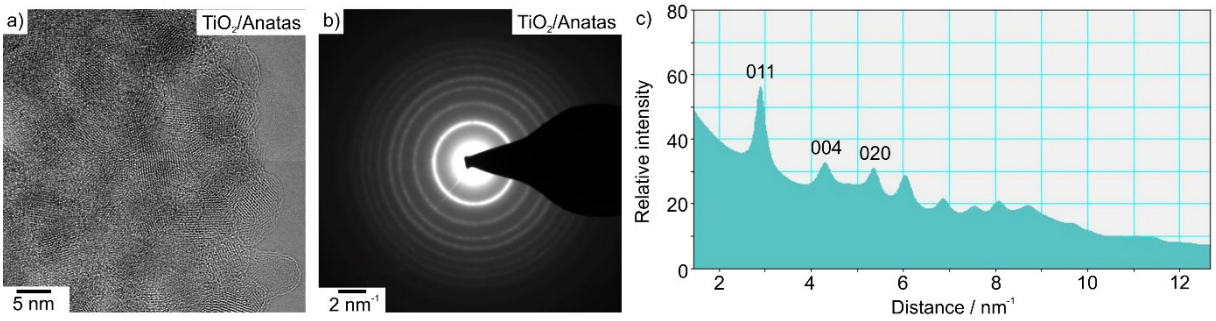

Figure S19. Crystallinity and phase analysis of the TiO_2-Pt HNS (0.7 wt-%) after sintering (300 °C, N_2): a) HRTEM of crystalline TiO_2 domains; b) SAED of crystalline TiO_2 domain; c) SAED pattern of crystalline TiO_2 domain, which can be indexed as anatase.

In regard of the sintering of the TiO_2-Pt HNS, finally, it is noteworthy that size and size distribution of the Pt nanoparticles are stable up to 300 °C, still showing many Pt nanoparticles of 3-4 nm in size (Figures S15,S16; *see main paper: Figure 6a-e*). A noticeable growth of the Pt nanoparticles to 4-7 nm was actually only observed >400 °C (Figure S20). After heating to 400 °C, the size and distribution of the Pt nanoparticles over the TiO_2 HNS nevertheless remains very uniform.

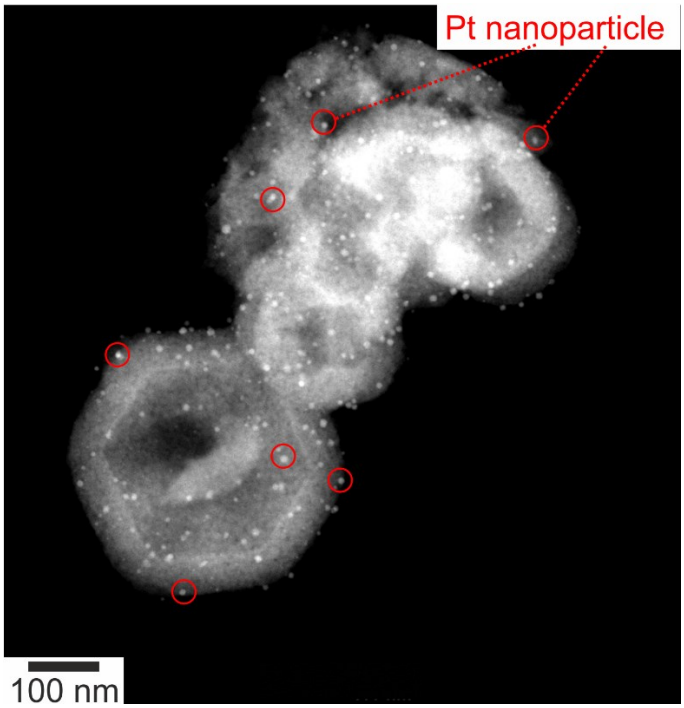

Figure S20. TiO_2-Pt HNS (0.7 wt-% Pt) for CO oxidation after sintered at 400 °C in nitrogen showing increased Pt nanoparticles (indicated by red circles) in comparison to sintering at 300 °C (see Figures S15,S16).

To examine the presence and oxidation state of platinum before and after the catalytic cycles, *ex situ* X-ray Absorption Near Edge (XANES) spectra was performed (Figure S21). Spectra were collected before and after the light-off/light-out CO oxidation cycles and indicate the presence of slightly more oxidized Pt after the catalytic cycle. According to a linear-combination fitting analysis slightly more oxidized Pt was observed at the end of the catalytic test (70% of the sites present as Pt(0)). The results of the XANES measurement align very well with the sample treatment history, since the as-prepared catalyst was reduced at 300 °C prior to the CO oxidation measurement. In regard of the XANES data, however, it needs to be noticed that the low Pt concentration limits the quality of data, so that the differentiation of Pt(0) and Pt(II) is difficult. Since the as-prepared TiO_2-Pt catalysts were pre-reduced by reducing-gas

treatment, equilibration between Pt(0) and Pt(II) might occur only during CO oxidation and result in a higher Pt(II) content.

The *ex situ* XAS measurements were performed in fluorescence mode at the KIT Synchrotron (CAT-ACT beamline)[S1] at the Pt L_3-edge (11,564 keV) using a Si (111) monochromator. The obtained data were quantitatively evaluated with ATHENA software 41[S2] by linear combination fitting (LCF). For the LCF analysis, spectra of a metallic Pt and PtO_2 were used as references in the fitting range of 11,540-11,600 keV.

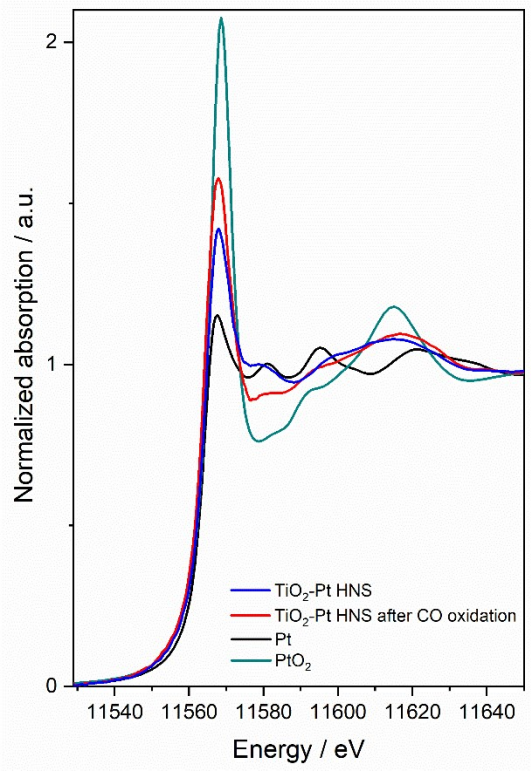

Figure S21. *Ex situ* XANES spectra collected at the Pt-*L3* edge for TiO_2-Pt HNS (0.7 wt-%) catalyst before (blue curve) and after catalytic CO oxidation (red curve) with XANES spectra of PtO_2 and Pt as references.

References

[S1]A. Zimina, K. Dardenne, M. A. Denecke, J. D. Grunwaldt, E. Huttel, H. Lichtenberg, S. Mangold, T. Pruessmann, J. Rothe and R. Steininge. *J. Phys.*, 2016, **712**, 23.

[S2]B. Ravel and M. Newville, *J. Synchr. Rad.*, 2005, **12.4**, 537.